Numerical Investigation of Beam-Column Connections in Precast Concrete Buildings

Ziyad Al-Gaboby [1]

Safwan Al-Sumaini [2]

[1] Assistant Professor, Civil Engineering Department, Faculty of Engineering, University of Science and Technology, Yemen. Email. ziyad90@gmail.com

[2] Assistant Lecturer, Civil Engineering Department, Faculty of Engineering, University of Science and Technology, Yemen. Email: safwan1906@gmail.com

https://doi.org/10.20428/JST.26.1.1

Numerical Investigation of Beam-Column Connections in Precast Concrete Buildings

Abstract:

The progressive collapse of structures has been the concern of many researches. Efforts have been made to develop methodologies of analysis and design for the mitigation of progressive collapse. Precast structures are more sensitive to progressive collapse than monolithic cast-in-situ reinforced concrete (RC) buildings because they poor continuity in the structural load paths. In this paper, Analytical study has been conducted to develop a non-linear finite element model (FEM) using ABAQUS 6.12 software to investigate the behavior of precast non-prestressed RC beam-column joint in case of sudden middle column removal. The non-linear behavior of concrete and steel is considered by the FEM. In addition, it takes into account the contact properties between surfaces at joints. A calibration was performed between the numerical and the experimental results, using three half-scale specimens tested under mid column lose, to verify that the FE model could be used for simulating precast beam column connections. There was a good agreement between experimental and FEM results.

Keywords: Precast frame, Beam-column joint, Investigation, Finite element analysis, Interface element, ABAQUS.

https://doi.org/10.20428/JST.26.1.1

المحاكاة الرقمية للاتصال بين العمود والجسر الخرساني للمباني مسبقة الصب

الملخص:

اهتمت العديد من الدراسات بالانهيار المتتالي للهياكل الانشائية والتي سعت الى تطوير منهجيات التحليل والتصميم التي تحد من الانهيار المتتالي. ونظرًا لأن الهياكل مسبقة الصب تضعف فيها الاستمرارية الهيكلية لمسارات الأحمال، فهي أكثر استجابة للانهيار المتتالي من المباني الخرسانية المسلحة المصبوبة في الموقع. في هذا البحث تم إجراء دراسة تحليلية لتطوير نموذج غير خطي بطريقة العناصر المتناهية باستخدام برنامج ABAQUS 6.12 لفحص سلوك الاتصال بين عمود وجسر خرساني مسلح غير مسبق الإجهاد في حالة الإزالة المفاجئة للعمود. يحاكي نموذج العناصر المتناهية السلوك الغير خطي للخرسانة والفولاذ. بالإضافة إلى ذلك، فإنه يأخذ في الاعتبار خصائص الاتصال بين الأسطح في المفاصل. تم إجراء معايرة بين النتائج الرقمية والمعملية باستخدام ثلاث عينات بمقياس النصف والتي تم اختبارها في منتصف العمود المفقود، للتحقق من أنه يمكن استخدام نموذج العناصر المتناهية لمحاكاة الارتباط بين العمود والجسر مسبقة الصب. اظهرت النتائج تطابق جيد بين النتائج التجريبية والرقمية.

الكلمات المفتاحية: الخرسانة مسبقة الصب، اتصال العمود بالجسر، عنصر الاتصال طريقة العنصر المتناهية الأباكوس.

1. Introduction

Over the most recent couple of decades, precast construction has turned out to be common in the world because of its advantages of construction. Precast structures are more potential to progressive collapse than cast-in-place monolithic buildings as a result of the lack of structural continuity and redundancy in the load paths. Therefore, it is critical to investigate performance of precast RC structures for progressive collapse to avert cataclysmic occasions such as the loss of one or more columns.

Numerous researchers have investigated the performance of various types of precast RC beam-column connections [2- 5].

Using non-linear FEM, Hawileh et al. [6] investigated the effect of cyclic loads on precast hybrid beam-column joints. Three dimensional (3D) solid elements were used for modeling precast posttensioned RC beam-column connection and surface-to-surface contact elements were used to represent the interaction between the beam and column faces. Their past experimental test results were used to validate the model response.

Under a column-loss scenario, Nimse et al. [11] evaluated the behavior of three various types of 1/ 3-scale precast beam-column connections. Monolithic specimens were evaluated for comparative purposes. Different joint details were used to build precast RC beam-column joints. The load-displacement characteristics of test specimens were used to evaluate their performance. The authors contended that the precast connections had higher peak load and ductility than monolithic joints.

Alrubaidi [1] experimentally investigated the performance of precast frames subjected to middle column-loss scenarios. Beam to column were joined together with corbel and cast-in dowel connection. The precast frames were tested to failure under a high-rate loading (100 mm/s) in order to simulate column-removal scenario. The behavior of different precast frames was assessed and compared in terms of mode of failure and load-displacement characteristics.

The main goal of this study is to develop a FEM using ABAQUS 6.12 [10] to simulate the performance of precast RC beam-column joints under middle column-loss scenario. The developed FEM takes into consideration the non-linear behavior of concrete, steel, and contact interaction between surfaces. Experimental test results done by Alrubaidi [1] were used to validate the FEM results.

https://doi.org/10.20428/JST.26.1.1

2. Experimental Program

In order to achieve the main goal of this study, the experimental data in the study of Alrubaidi [1] has to be obtained and then utilized for FEM validation. Table 1 and Fig. 1 show and describe the details of the experimental tests for beam, column, mild-steel bar, and reinforcement.

Table 1: Experimental details of precast frames used for FEM validation [1]

Type	Beam details (mm)		Column details (mm)		Type of connection	Corble details (mm)	Type of strengthened system
	b x h x L	Reinforcement	b x h x H	Reinforcement			
Specimen PC-C	350x350x2620	4ϕ16 mm Top 4ϕ16 mm Bottom Stirrups ϕ8 @ 100 mm c/c	350x350x1750	8ϕ16 mm longitudinal Stirrups ϕ8 @ 100 mm c/c	Precast with grouting of corbel rebar	350 × 250	
Specimen PC-S	350x350x2620	4ϕ16 mm Top 4ϕ16 mm Bottom Stirrups ϕ8 @ 100 mm c/c	350x350x1750	8ϕ16 mm longitudinal Stirrups ϕ8 @ 100 mm c/c	Precast with grouting of corbel rebar	350 × 250	strengthened using CFRP combined with NSM within connection region

Table 2: Material properties of precast frames used for FEM validation [1]

Material	Properties
Concrete	Poisson ratio = 0.2
	Compressive strength = 37.3 MPa
	Modulus of elasticity = 28704.7 MPa
	Density = 2.4 e^{-9} ton/mm3
CFRP	Type of FRP= Unidirectional CFRP sheet
	Elastic modulus in primary fibers direction = 77.3 GPa
	Elastic modulus of CFRP 900 to primary fibers= 40.6 MPa
	Fracture strain =1.1%
	Ultimate tensile strength = 846 MPa
	Thickness per layer = 1.0 mm

Table 2: Continued

Material	Properties
Reinforcing steel	Poisson ratio = 0.3
	Yield stress = 525 MPa
	Modulus of elasticity = 200000 MPa
	Density = 7.8 e^{-9} ton/mm^3

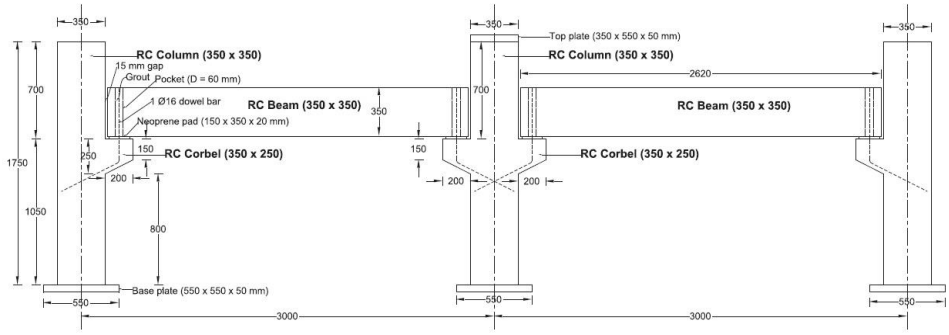

(a)

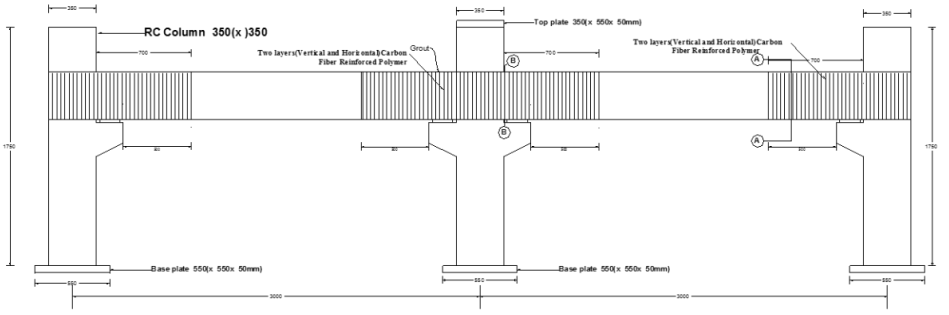

(b)

Figure 1: Concrete dimension of tested specimens [1]
(a) specimen PC-C, (b) Specimen PC-S

3. Numerical Modeling

The most practical way to analysis a structure consisting a large number of degrees of freedom is the FEM. Finite element analysis can be performed by a number of commercial programs. In this research the non-linear finite element software ABAQUS 6.12 was used for creating the 3D FEM. Experimental tests can be perfect method to investigate the behavior and failure of precast RC structures. They may, however, be costly and time-consuming. They need adequate facilities, space, test setup, and personnel. Computational models, if done correctly, might be a viable choice in contrast to the expensive experimental investigation.

https://doi.org/10.20428/JST.26.1.1

3D FEMs of precast RC frames with and without strengthening schemes have been modeled in ABAQUS 6.12 according to Alrubaidi [1] as shown in Fig. 2.

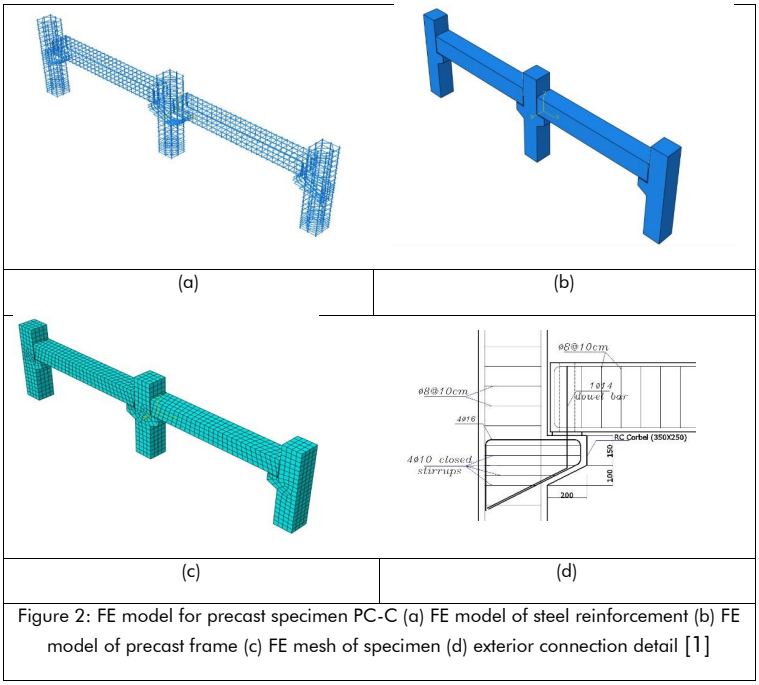

Figure 2: FE model for precast specimen PC-C (a) FE model of steel reinforcement (b) FE model of precast frame (c) FE mesh of specimen (d) exterior connection detail [1]

3.1 Materials

3.1.1 Concrete

The plastic-damage model in ABAQUS 12.6 was used to simulate the behavior of concrete material used in beams and columns.The model is based on the developed models by Lubliner et al [9] and By Lee and Fenves [8]. The plastic-damage model can be used to evaluate non-linear behavior of concrete including failures (crashing and cracking) in both compression and tension under external loading.

The damage plasticity model for concrete (which is a continuum, plasticity-based) assumed that concrete›s two major failure modes are crushing in compression and cracking in tension [8,9].

Concrete Damaged Plasticity model (CDP) uses a yield condition based on the yield function proposed by J. Lubliner et al. [9] and it also includes the modifications model proposed by Jeeho Lee and Gregory L. Fenves [8] to determine different evolution of the concrete strength under compression

and tension. compression. Where p is refer to hydrostatic pressure, q is refer to the Mises equivalent stress, s is refer to the stress deviator, y and α are dimensionless material properties, $\hat{\sigma}_t(\tilde{\varepsilon}_t^{pl})$ and $\hat{\sigma}_c(\tilde{\varepsilon}_c^{pl})$ are tensile and compressive cohesion stresses respectively, as shown in Fig. 3.

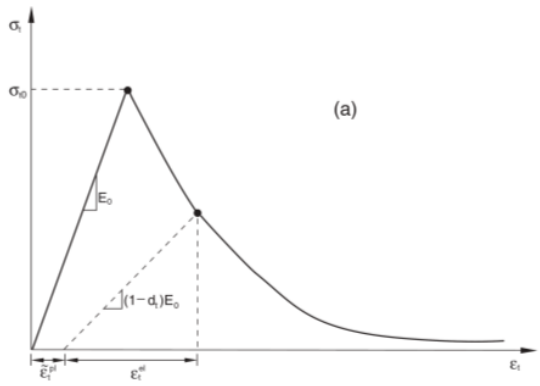

Figure 3: Yield surface in plane stress [10]

The α coefficient can be calculated from σb0 the biaxial initial yield compressive stress and σ_{c0} uniaxial initial yield compressive stress, Typical experimental values of stress are $1.1<(\sigma_{bo}/\sigma_{co})<1.16$ and yielding values are $0.08<\alpha<0.12$ [9], β it can be determined from the effective compressive and tensile cohesion stresses.

The damaged in compression and tension are depended on two hardening variables. The hardening variables are equivalent plastic strains in tension $\varepsilon_t^{\sim pl}$ and compression $\varepsilon_c^{\sim pl}$. Increasing values of these variables reflect crushing and micro-cracking in the concrete model, and the hardening variables control the evolution of the yield surface.

The stress-strain relation under uniaxial loading is represented by the concept developed by Lee and Fenves [8]:

$$\sigma_t = (1-d_t)E_0(\varepsilon_t-\varepsilon_t^{\sim pl}) \qquad 1$$

$$\sigma_c = (1-d_c)E_0(\varepsilon_c-\varepsilon_c^{\sim pl}) \qquad 2$$

The degraded response of concrete is described by d_c and d_t, which are referred to independent uniaxial damage variables for compression and tension, respectively. Moreover, d_c and d_t are assumed to be functions of the temperature, plastic strains, and field variables. The d_c and d_t parameter have values ranging from 0 to 1 ($0 \leq d < 1$).

https://doi.org/10.20428/JST.26.1.1

The CDP model assumes that the response of concrete for uniaxial compressive and tensile is described by damaged plasticity, as shown in Fig. 4.

The CDP model is a modification of the Drucker–Prager theory. Based on the modifications, the yield surface in the deviatoric plane does not need to be a circle (as for the Drucker-Prager model), and it is also influenced by Kc parameter, as shown in Fig. 5.

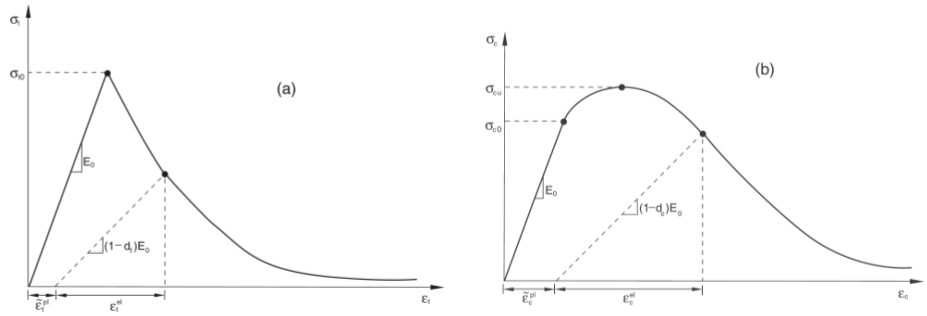

Figure 4: The stress-strain relations for concrete to uniaxial loading (a) In tension (b) In compression [10]

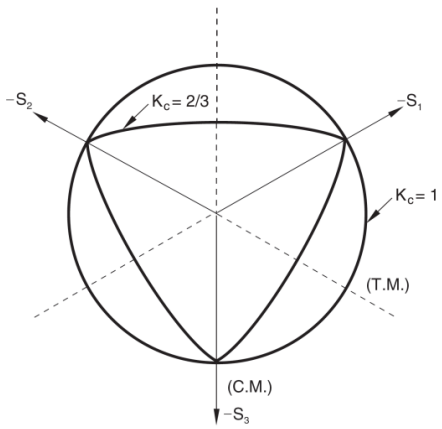

Figure 5: Yield surfaces in the deviatoric plane [10]

The CDP model using non-associated potential flow follows the Drucker–Prager hyperbolic as shown in Fig. 6. The shape was adjusted through the eccentricity parameter ϵ, it is a small value that characterizes the rate of approaching the hyperbola plastic potential to its asymptote. Where ψ is the dilation angle, which is measured in the p-q plane.

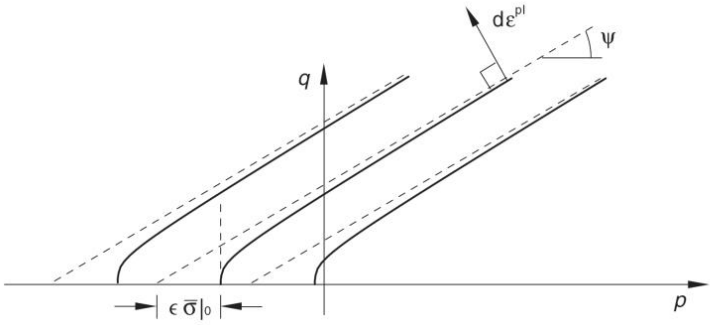

Figure 6: Hyperbolic Drucker–Prager flow potential [10]

CDP model can be improved by using viscoplasticity, which helps overcome convergence difficulties by defining the viscosity parameter with a small value.

The concrete compressive stress-strain curve obtained from the experimental test conducted by Elsanadedy et al. [7], as shown in Fig. 7.

The tensile stress-strain curve behavior for concrete is shown in Fig. 8. The response of concrete in tension is assumed to be linear with an increase in tensile strain up to tensile strength f_{ct}. After that, tensile stress decreased as a straight line to zero. Tensile strength f_{ct} for concrete was calculated equal 10% from compressive strength [12].

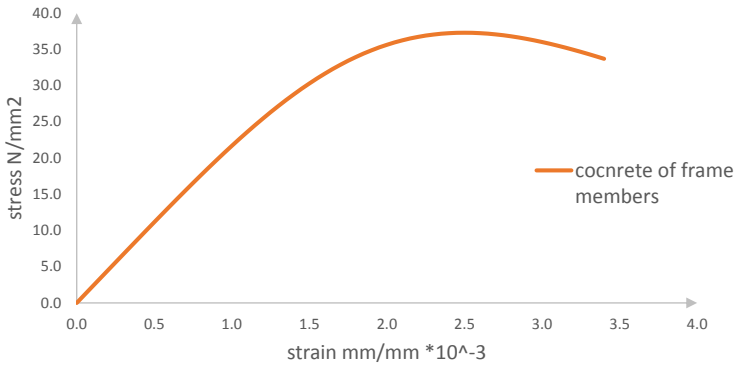

Figure 7: The concrete compressive stress-strain curve

https://doi.org/10.20428/JST.26.1.1

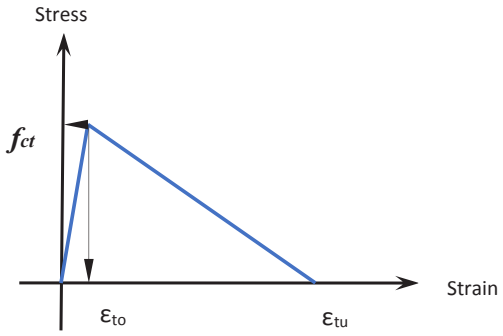

Figure 8: concrete tensile stress-strain curve

The parameters of CDP that were used for modeling concrete in ABAQUS, are shown in Tables 3.

Table 3: The parameters of CDP

Dilatation angle	Eccentricity	σ_{b0}/σ_{c0}	K	Viscosity parameter
7	0.1	1.16	0.67	0.00025

3.1.2 Reinforcement Bars

In order, to define the behavior of steel reinforcement in ABAQUS elastic and plastic properties are required. Fig.9 shows a typical stress-strain curve that would be useful for molding steel rebar behaviors in ABAQUS. Its yield point and its post-yield hardening are parameters that describe the plastic behavior of the material and required for modeling it.

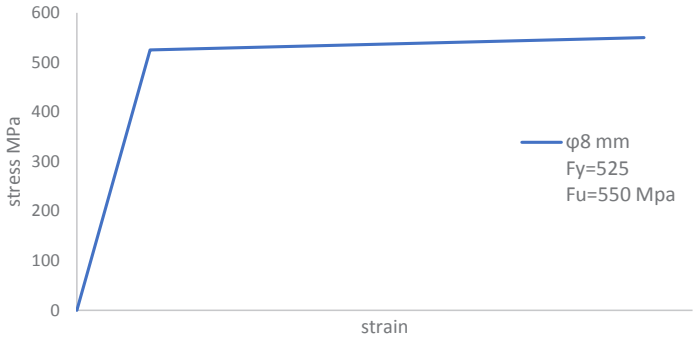

Figure 9: Idealized stress-strain relationship for reinforcing rebar material

3.2 Elements Type

In ABAQUS, there is a wide element library to provide a useful tool in modeling different structures and solving many types of problems. Those elements are categorized into the following types (family, degrees of freedom, number of nodes, integration and formulation) [10].

3.2.1 Concrete Elements

For non-linear analyses including plasticity, contact, and large deformations continuum elements in ABAQUS can be used. Many types of numerical techniques in ABAQUS can be used to integrate different quantities over the volume of each element, which allows complete flexibility in material behavior. Also, Gaussian quadrature can be used for evaluating the behavior of the material at each integration point for each element. In ABAQUS, continuum (solid) elements can use reduced or full integration, an option that have an important effect on the accuracy of the elements for a specific problem. Reduced integration reduces the consumed time for running, especially in 3D models. For example, C3D20R has only 8 (2x2x2) in each direction integration points, while C3D20 has 27 (3x3x3) integration points, therefore C3D20 element is approximately more than C3D20R element 3.5 times. The difference between element types is shown in Fig. 10. The (C3D20R) element, 20-node quadratic element with reduced integration, was used for modeling the concrete (beams, columns).

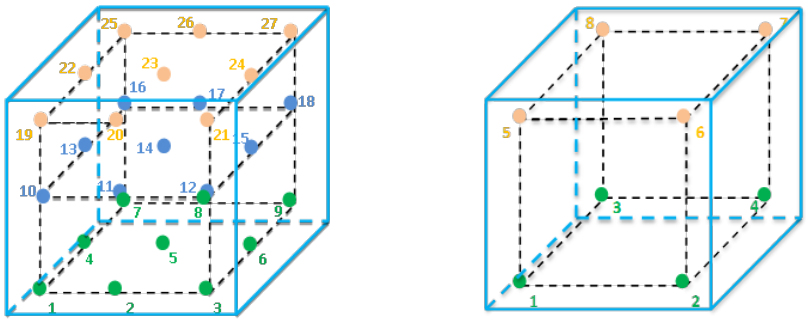

(a) **(b)**

Figure 10: Integration point for elements (a) C3D20 and (b) C3D20R

3.2.2 Reinforcement Bars Elements

Truss elements in 3D was the second type of elements that were used in FE modeling. It was used for modeling steel reinforcement, which support loading along the axis of the member. Truss element (T3D2), which is a 3D truss element with two nodes, was used for modeling reinforcement bars that was embedded in concrete members.

https://doi.org/10.20428/JST.26.1.1

3.2.3 Interface Elements

The interface element used here tends to act as a bond between "Concrete-to-CFRP" and to provide easily the interface damage formation. For modeling CFRP/Concrete interface in ABAQUS cohesive elements were used for the mesh elements of the bond. Regarding the modeling of interface in FRP-to-concrete, the constitutive reaction of cohesive components may be easily defined using the traction-separation rule obtained from fracture mechanics. In this study, a traction-separation law is used to represent the interface›s bond behavior. The cohesive element's response is considered to be linear. The failure mechanism is composed of two ingredients: a damage evolution law and a damage initiation criterion. In the traction-separation rule, the initial response is the climbing linear segment up to the damage initiation criterion. The maximum traction is used by the damage initiation criterion to describe the beginning of the interface response deterioration. The fracture energy required to separate the interface is equal to the area under the traction-separation response.

If the cohesive zone is exceedingly thin, and may be assumed to be of zero thickness for all practical purposes, the constitutive reaction is often defined in terms of a traction-separation rule [10].

When the maximum nominal stress ratio reaches a value of one in the current finite element analysis utilizing cohesive elements, damage is predicted to begin. The following equation depicts the failure start law necessary to stimulate interface layer damage corresponding to the maximum nominal stress criteria.

$$3\max\left(\frac{t_n}{t_n^o}, \frac{t_s}{t_s^o}, \frac{t_t}{t_t^o}\right)=1$$

Where t_n, t_S and t_t are the maximum stresses for normal, and maximum shear in two directions, respectively; t_s°, t_t°, and t_n° refer to peak shear failure in two directions and the peak normal failure strengths, respectively.

3.3 Constraints & Interactions

3.3.1 Embedded Elements

For modeling interaction between concrete and reinforcement rebar ABAQUS has offered a tool (embedded element) that can be used for modeling a reinforcement inside concrete.

An embedded constraint can be utilized to embed a model region within a «host» model region or the whole model. Longitudinal rebar, stirrups and tie rebar were simulated using truss element [10].

3.3.2 Interactions

In ABAQUS, to define interaction between members and elements there are different methods. The first method is contact pairs (surface to surface); it is used for defining the interaction between two or more surfaces. The second method (self-contact) is used to simulate a single surface that interacts with itself, furthermore it can define interactions between members. ABAQUS features a variety of contact formulations, each of which is determined by the amount of options available, which include contact discretization, assigning slave and master roles to contact surfaces, and using a tracking technique.

In the contact restrictions region, surface-to-surface discretization takes into account the form of both the master and slave surfaces. Instead of enforcing contact criteria at individual slave nodes, the surface-to-surface tool enforces them in an average sense over regions near slave nodes. Traditional node-to-surface discretization establishes contact conditions such that each slave node on one side of a contact interface effectively interacts with a point of projection on the opposite side on the master surface of the contact interface, with the averaging regions roughly centered on slave nodes [10].

The way touch surfaces interact will be greatly influenced by a tracking strategy. There are two tracking algorithms in ABAQUS for calculating relative motion for interaction surfaces. The first is finite sliding, which enables any arbitrary motion of the surfaces and is the most generic. The second is small sliding, two bodies may be subjected to large motions, however it assumes there will be relatively little sliding. In ABAQUS cannot be assigned the cohesive behavior in the contact pairs using the surface-to-surface discretization and the finite sliding tracking approaches.

In this research, a surface-to-surface discretization was used for modeling the contact between members. One surface was designated as the master and the other as the slave for each contact pair.

With a node-to-surface contact formulation, the choice of master and slave often has an impact on the results as depicted in Fig. 11.

That whenever a bigger surface comes into touch with a smaller surface, it›s ideal to make the larger surface the master and the smaller surface the slave.

https://doi.org/10.20428/JST.26.1.1

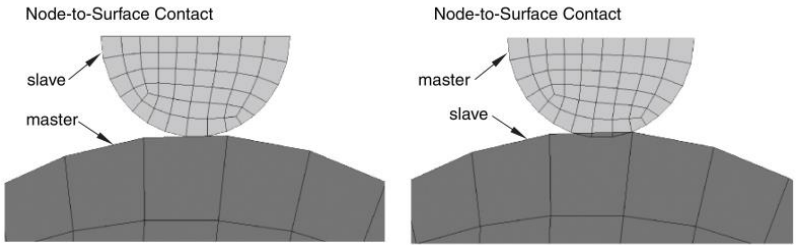

Figure 11: Effect of slave-master assignments on node-to-surface [10]

3.3.3 Contact Properties

The contact interaction between surfaces is specified by specifying a contact property model. The relationship pressure-overclosure that controls the motion of the surfaces, a cohesive behavior that is used for modeling the behavior of adhesive joints, and a friction model that specifies the resistance tangential motion in the surfaces are all examples of mechanical contact property models [10].

The hard contact model was used to characterize the relation between pressure-overclosure in this study›s models. Penetration is not allowed at each limitation position in a hard contact, and the magnitude of contact pressure that can be transmitted between the contact surfaces has no limit.

In this research, the coefficient of static friction of 0.6 between concrete surfaces was used in contact property model, whereas the friction coefficient of 0.4 was used between concrete and neoprene pads surfaces in contact property model.

In ABAQUS, cohesive behavior is defined as part of the interaction properties assigned to the contact surfaces.

Table 4: The interface zone's characteristics

Parameter	υ	Knn (MPa)	Kss = Ktt (MPa)	t_n^f (MPa)	$=t_t^f\ t_s^f$ (MPa)
Value	0.33	2000	1500	60	80

3.4 Boundary Condition and Load Application

Finite element models are largely dependent on the speed of loading. When a building is subjected to blast loading, a column may be suddenly removed, resulting in the structure›s progressive collapse. This phenomenon was simulated by applying a 100 mm/s velocity boundary condition for the middle column at a mid-point in the upper surface of the middle column and

boundary conditions for nodes at the bottom surface of the middle column was free as shown in Fig. 12. During the analysis, the overall loading time was four seconds. All nodes at the bottom surfaces of external columns are restricted in all degrees of freedom (i.e., fixed).

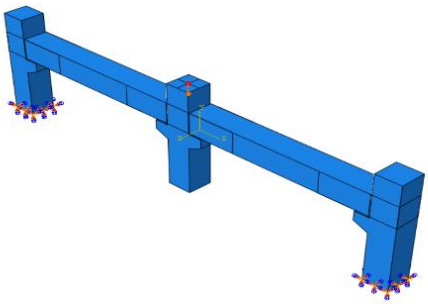

Figure 12: Boundary Condition and Load Application

4. Validation of FE modeling

The result of numerical modeling and the experimental results [1] have been compared to ensure that FE models in ABAQUS are capable of simulating PC frames that have a behavior similar to experimental specimens. The numerical study›s findings are described in sub-sections.

4.1 Failure Mode

The final failure modes of for specimen's PC-C and PC-S are depicted in Fig.13, respectively, as obtained by the findings of the FEM analysis. It is seen from these figures that there is a good agreement between FEM and experimental modes of failure for PC-C and PC-S frames. Following the study, it was discovered that PC-C frame exhibited proper hinge behavior. Both beams of specimen PC-C rotated at their ends during the analysis until the internal ends came into contact with the center column, and the mechanism of failure at the ultimate was due to crushing of concrete at the inner beam-column joint, as shown in Fig. 13. (a). No further damage was found in any of the PC-C›s frame including columns and beams.

Fig. 13(b) shows comparison modes of failure for FEM and experimental [1] of PC-S specimen, which was strengthened using NSM steel bars combined with CFRP sheets at the beam-column joints. A good agreement was noticed between the FEM and experimental in terms of modes of failure for PC-S frame. Due to fracture of extreme bottom NSM bars combined with rupture of horizontal CFRP laminates at the bottom edge at the column face, failure of

https://doi.org/10.20428/JST.26.1.1

PC-S1 specimen began in the beam surrounding the internal beam-column connections as shown in Fig. 13(b).

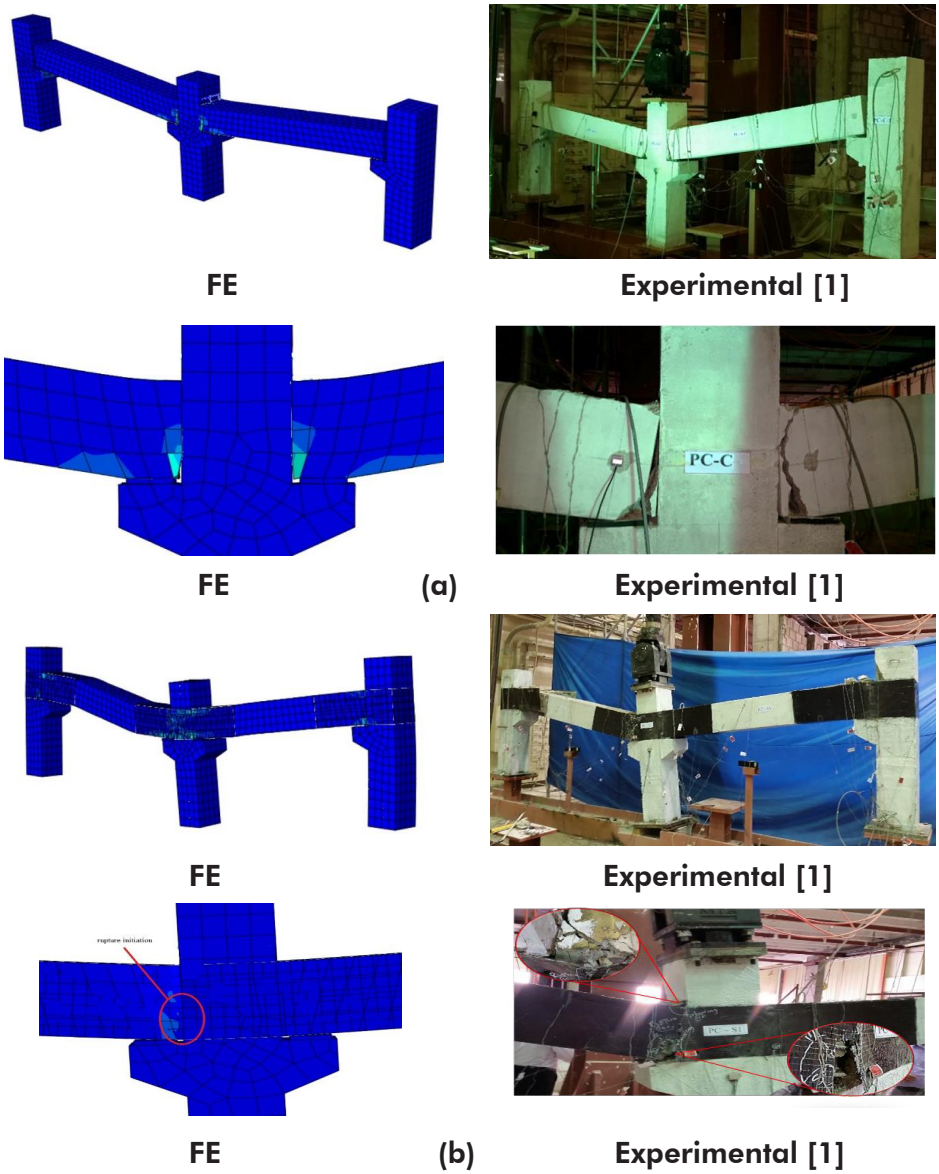

Figure 13: Comparison of failure modes of experimental and FEM of frame and middle connection of: (a) PC-C frame; (b) PC-S frame

4.2 Load-displacement characteristics

From numerical and experimental research [1], a comparison of load vs. middle column displacement was derived for the two test frames. The numerical and experimental load-displacement curves demonstrate good agreement, notably for the peak load as shown in Fig. 14.

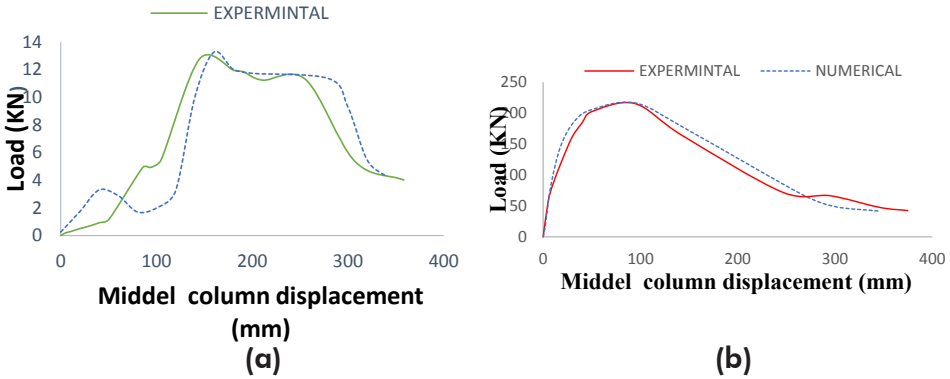

Figure 15: Comparison of FEM and experimental [1] in terms of load-displacement curve for: (a) PC-C frame; (b) PC-S frame

Table 5 presents the comparison results of load-displacement characteristics. As illustrates in Table 5, difference of 0.04.0%- is noticed between the peak loads of FEM and experimental peak loads. Nevertheless, variations of 29-percent, 1215- percent, and 46- percent were reported for displacement at peak load in the middle column, displacement at peak load in the beam mid-span, and displacement at ultimate condition in the middle column, respectively, when compared to experimental findings.

Table 5: Comparison of load-displacement characteristics for FEM and experimental results [1]

Specimen ID	Result	p_u(KN)	p_Y(KN)	$\Delta_{u,c}$(mm)	$\Delta_{u,b}$(mm)	Δ_y(mm)	Δ_u(mm)
PC-C	EXP.	13	NY	145	66	NY	265
	FE	13.5		160	75		251
	EXP/ FE	0.96		0.91	0.88		1.06
PC-S	EXP.	215.6	151	97	41	26	135
	FE	216.4	154	95	48	24.5	130
	EXP/ FE	0.996	0.98	1.02	0.85	1.06	1.04

p_u= peak load, $\Delta_{u,c}$= middle column displacement at peak load, $\Delta_{u,b}$= displacement at peak load in mid-span, p_y= load at yielding of beam bottom reinforcing rebar, Δ_y= middle column displacement at yielding of beam bottom reinforcing rebar, Δ_u= displacement of middle column at ultimate

https://doi.org/10.20428/JST.26.1.1

5. Conclusions

Based on comparisons between FEM analysis findings and experimental data [1], the following conclusions may be drawn:

- The FEM can be used to make accurate predictions behavior of other precast concrete frames joints duo to the good agreements between FEM and experimental in terms of load-displacement envelopes.
- The precast model PC-C, which was utilized for validation, was proven to be extremely vulnerable to progressive collapse due to low ductility and absence of structural continuity in beam-column connections, resulting in a lack of redundancies in the structural load paths. As a result, it is strongly recommended that they use CFRP with near-surface mounted bars and steel plates to strengthen their connection details.

6. References

[1] Mohammed A. Alrubaidi (2016) "Rehabilitation of beam column connection in existing precast concrete buildings for progressive collapse mitigation" MS Thesis, King Saud University.

[2] R. Vidjeapriya, K.P. Jaya, Experimental study on two simple mechanical precast beam column connections under reverse cyclic loading, J. Perform. Constr. Facil 27 (2013) 402–414.

[3] R. Vidjeapriya, K.P. Jaya, Behaviour of precast beam-column mechanical connections under cyclic loading, Asian J. Civil Eng. (Build. Hous.) 13 (2014) 233–245.

[4] H.K. Choi, Y.C. Choi, C.S. Choi, Development and testing of precast concrete beam-to-column connections, Eng. Struct. 56 (2013) 1820–1835.

[5] M.K. Joshi, C.V. Murty, M.P. Jaisingh, Cyclic behaviour of precast RC connections, Indian Concr. J. 79 (2005) 43–50.

[6] R.A. Hawileh, A. Rahman, H. Tabatabai, Nonlinear finite element analysis and modeling of a precast hybrid beam-column connection subjected to cyclic loads, Appl. Math. Model. 34 (2010) 2562–2583.

[7] Almusallam, T. H., Elsanadedy, H. M., Al-Salloum, Y. A., Siddiqui, N. A., & Iqbal, R. A. (2018). Experimental Investigation on Vulnerability of Precast RC Beam-column Joints to Progressive Collapse. KSCE Journal of Civil Engineering, 22(10), 3995-4010.

[8] Jeeho Lee and Gregory L. Fenves "Plastic-Damage Model for Cyclic Loading of Concrete Structures" Journal of Engineering Mechanics, vol. 124, no.8, pp. 892–900 (1998).

[9] J. Lubliner et al "A Plastic-Damage Model for Concrete" International Journal of Solids and Structures, vol. 25, pp. 299–329 (1989).

[10] Dassault Systèmes. ABAQUS Manual, Version 6.12, 2012.

[11] R.B. Nimse, D.D. Joshi, P.V. Patel, Behavior of wet precast beam column connections under progressive collapse scenario: an experimental study, Int. J. Adv. Struct. Eng. 6 (2014) 149–159.

[12] A.H. Nilson et al. "Design Of Concrete Structures", 14th edition, McGraw-Hill, United States (2010).

[13] ACI Committee 318, Building code requirements for structural concrete and Commentary. ACI 318-14, American Concrete Institute, Detroit, MI, USA, 2014.

https://doi.org/10.20428/JST.26.1.1